DTU Library

Towards the understanding of (dis)charging mechanism of VS_4 cathode for magnesium batteries

Jankowski, Piotr; Lastra, Juan Maria Garcia

Published in:
Journal of Energy Storage

Link to article, DOI:
10.1016/j.est.2023.106895

Publication date:
2023

Document Version
Publisher's PDF, also known as Version of record

Journal of Energy Storage 62 (2023) 106895

Contents lists available at ScienceDirect

Journal of Energy Storage

journal homepage: www.elsevier.com/locate/est

Research papers

Towards the understanding of (dis)charging mechanism of VS_4 cathode for magnesium batteries

Piotr Jankowski [a,b], Juan Maria Garcia Lastra [a,*]

[a] Department of Energy Conversion and Storage, Technical University of Denmark, Kgs. Lyngby 2800, Denmark
[b] Faculty of Chemistry, Warsaw University of Technology, Warsaw 00-661, Poland

ARTICLE INFO

Keywords:
Magnesium batteries
Cathodes
DFT
VS_4

ABSTRACT

Rechargeable magnesium batteries are promising energy storage technology which could eventually power electric cars. However, the double charge of Mg-ion results in sluggish kinetics in most cathode materials. Due to that, exotic materials, with more complex discharging mechanisms than what we are used for conventional Li-ion batteries, have been explored. In particular, vanadium tetrasulfide (VS_4), a quasi-1D material, was recently shown to be a good candidate for magnesium storage, providing good theoretical capacity and excellent kinetics for magnesium intercalation. Here we present a DFT-based analysis of the complex magnesation process of VS_4. The results indicate a mixed hetero- and homogeneous process with $Mg_{0.75}VS_4$ formed at the initial stages of the cathode discharge. At higher magnesiation levels (i.e., Mg_xVS_4 with $x > 1$) we observed a possible degradation mechanism related to the V—S bond breaking, which leads to the formation of magnesium sulfur clusters inside the structure. All of that enables us to identify the origin of the superior properties of VS_4 as cathode material, enabling the design of strategies to further improve its performance.

1. Introduction

Magnesium batteries are considered one of the most promising post-lithium technology, thanks to the exclusive nature of magnesium metal employed as anode: ultrahigh theoretical volumetric energy density (3833 mAh cm^{-3}), low electrochemical potential (−2.37 V *vs.* SHE), wide natural abundance and lower vulnerability for dendritic deposition [1–3]. However, to benefit from the superior properties of a magnesium anode, efficient cathode materials are required. Unfortunately, the double charge of magnesium cation usually leads to slow diffusion kinetics in the solid host [4]. Due to that, most well-known cathode materials used in Li- and Na-batteries are less efficient for magnesium intercalation/deintercalation. In particular, due to the strong interaction between Mg^{2+} cations and oxygen anions, oxides hinder cation mobility inside the material, completely preventing the deintercalation of Mg^{2+}. Sulfides have shown to be more suitable, as sulfur ligands show lower polarizability than oxygen ligands, resulting in a weaker coulombic attraction with guest Mg^{2+} ions [5], which leads to both high cation mobility and facile (de)solvation at electrode/electrolyte interface. Thus, many sulfide-based materials have been proposed and studied for magnesium batteries, including TiS_2, VS_2, MoS_2, and Mo_3S_4, with the latter, namely Chevrel Phase (CP), being so far the best performing magnesium cathode material. The excellent diffusion properties of CP are partially related to a large number of vacant sites where magnesium cation can site, resulting in a highly disordered structure [6]. Unfortunately, the amount of magnesium that CP can host is limited by 1 mol per Mo_3S_4 formula, giving quite a low capacity of 130 mAh g^{-1}. In addition, the potential in CP is only 1.2 V *vs.* Mg.

Recently, another sulfide material, vanadium tetrasulfide – VS_4, has brought attention to its application in multivalent batteries [7–9]. In detail, the VS_4 structure consists of atomic-chain nanorods composed of V^{4+} ions coordinated to sulfur dimers (S_2^{2-}), which are loosely stacked and bonded to each other by weak van der Waals forces (Fig. 1). A large interchain distance, 5.83 Å, offers abundant active sites for cation diffusion and storage. Moreover, a narrow bandgap, below 1.0 eV, provides relatively high electronic conductivity to the material [8]. These properties made VS_4 very attractive as a cathode for many types of batteries.

Theoretical studies of VS_4 revealed its peculiar electronic structure with extensive overlap of the sulfur (sp) bands with the vanadium (d) orbitals [7]. As a result, the reduction/oxidation process becomes complex. In conventional insertion cathodes, two redox behaviors are

* Corresponding author.
E-mail addresses: piotr.jankowski1@pw.edu.pl (P. Jankowski), jmgla@dtu.dk (J.M.G. Lastra).

https://doi.org/10.1016/j.est.2023.106895
Received 20 December 2022; Received in revised form 26 January 2023; Accepted 11 February 2023
Available online 20 February 2023

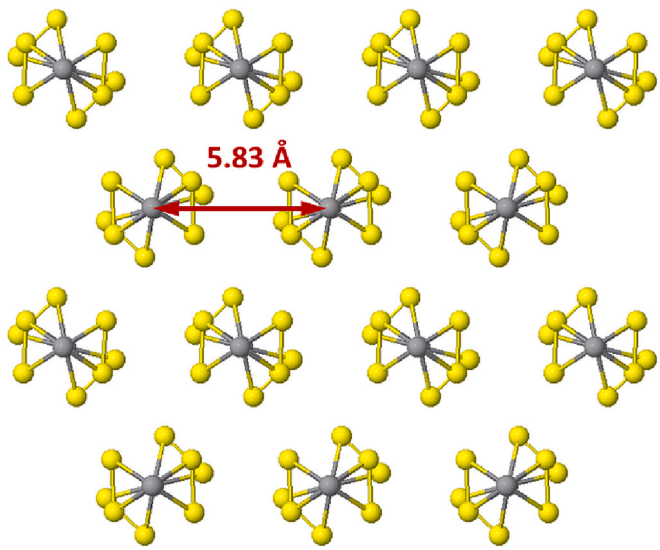

Fig. 1. Structure of VS_4 cathode material.

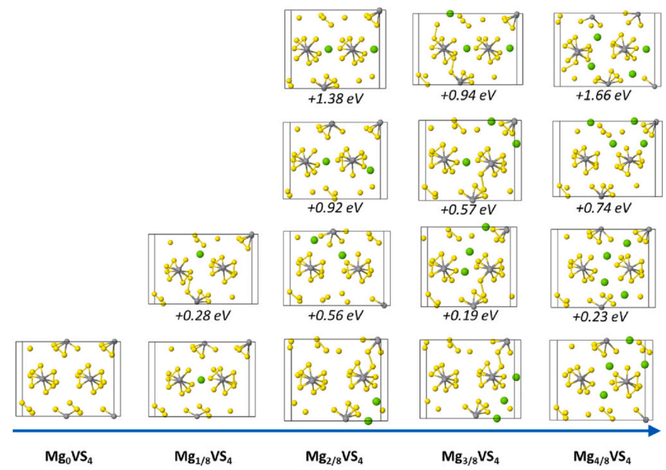

Fig. 2. Some representative structures of MgxVS4. The structures at the bottom are the most stable at different degrees of magnesiation. The cell presents 8 VS_4 formula units. The energies are relative to the ground state energy at a given degree of magnesiation. Energies differences correspond to the supercells containing 8 VS_4 formula units.

typically observed, namely: i) the insertion (extraction) of cations produces a reduction (oxidation) reaction in the transition metal atoms or, ii) alternatively, anions may get oxidized upon the extraction of cations (i.e., the so-called anionic centered redox processes present in Li-rich oxides [10,11] and some sulfides [12]). In some cathode materials, either a cation redox process or an anionic redox process occurs depending on the state of charge. In VS_4 the situation turns out more complicated: Britto et al. and Li et al. both showed that upon intercalation of lithium or magnesium cations into VS_4, respectively, reduction of disulfides is surprisingly accompanied by the oxidation of vanadium cation towards V^{5+} [7,13]. Additionally, the reduction of disulfide ligands induces their dissociation and some structural changes in the material. In our previous study, we have already shown that the opening and closing of sulfur dimers further support the diffusion of magnesium cation inside VS_4, similar to chain movements in solid polymer electrolytes [7]. All these processes together result in a very specific mechanism of cation storage in VS_4. Although a detailed analysis has already been performed for the lithium system [13–20], experimental results suggest no direct analogy for the magnesium one [7,9,21]. Unlike in the case of Li^+ intercalation, no significant changes in the cathode structure are observed upon cycling using XRD techniques. The magnesiation of VS_4 [V^{4+}; S_2^{2-}] is limited by the formation of $Mg_{1.5}VS_4$ [Mg^{2+}; V^{5+}; S^{2-}], and further reduction towards V^0, as during lithiation, becomes unfeasible. The Mg-VS_4 compositional space has already been explored up to $Mg_{0.875}VS_4$ by Wang et al. [8], but without considering the crucial phase stability and ignoring the region of high magnesium concentration – important for understanding the irreversibility observed during the first cycles [7,9]. Thus, here we further examine the Mg^{2+} storage properties of VS_4 cathode by DFT calculations with a focus on the magnesiation mechanism and the instability at high magnesium concentrations.

2. Methodology

All DFT electronic structure calculations were performed using Vienna ab-initio Simulation Package (VASP) [22], following methodology established before for VS_4 [7]. All calculations employed SCAN exchange-correlation functional [23] and projector augmented wave (PAW) potentials for all elements [24]. The application of a more accurate exchange-correlation functional than PBE was shown necessary for this system in previous works [7]. This makes the analysis presented here more accurate compared to other studies [8]. An energy cut-off of 520 eV was imposed for the plane-wave basis. The supercell of VS_4 was constructed from the primitive cell by doubling the system, comprising eight units of VS_4. A Gamma-centered $3 \times 3 \times 5$ k-mesh grid was used. The initial structures at different magnesium concentrations were constructed by placing magnesium cation with a randomized algorithm to fully explore possible geometries. For that, the Pymatgen package has been used to determine the sites to place Mg. [25] Thereafter a Python script randomly chooses between the Mg sites imposing the following conditions: (i) the distance between any two magnesium cations must be larger than 1.5 Å, (ii) and distance between a new magnesium and a sulfur atom must be lower than 2.5 Å (to induce coordination). At least 25 geometries were generated for each concentration, from 1 to 12 magnesium atoms in the unit cell. The optimization of the geometry was performed in several steps, to avoid the destruction of the VS_4 structure due to extremally high initial forces (Fig. S1): (i) first, the positions of vanadium atoms were blocked, together with distances between vanadium and sulfur – allowing for optimization of the magnesium coordinates, together with dynamic dissociation of disulfide ligands until forces reached 0.8 eV $Å^{-1}$; (ii) second, the cell volume has been optimized, allowing for expansion due to cations intercalation, with the convergence criteria set at 0.5 eV $Å^{-1}$; (iii) the structure inside the cell was optimized, keeping vanadium atoms at blocked positions; for the systems at higher magnesiation state (above $Mg_{8/8}VS_4$) an additional Hookean constrain has been introduced, imitating a weak spring between sulfur and the closest vanadium atom to prevent the breaking of the bond; this step was performed until forces reached 0.2 eV $Å^{-1}$; (iv) for the final step, all constraints have been removed, as well as cell parameters were optimized using a force convergence criteria of 0.03 eV $Å^{-1}$. Over 500 structures have been constructed and optimized to provide a good picture of the system. Two convex hull plots [26] were generated, taking as a reference for the discharged state of the cathode $Mg_{8/8}VS_4$ and $Mg_{12/8}VS_4$, respectively. In both cases, we took VS_4 as a reference for the fully charged cathode, considering only the structure that preserved all V—S bonds. The scans of the V—S bond length have been performed for the lowest energy structure, selecting the V—S bond with the largest initial length [27]. The distance between selected atoms was blocked, and all other parameters reoptimized at each step of the scan, changing the bond length in steps of 0.05 Å. The charge assignment to the atoms was performed using Bader Charge Analysis [28].

3. Results & discussion

To accurately determine the transformations of VS_4 during

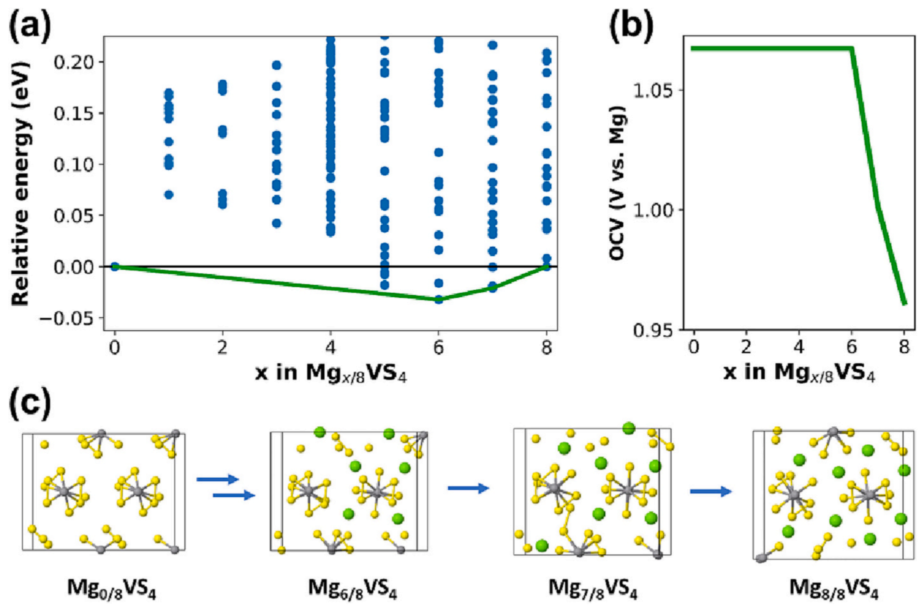

Fig. 3. (a) Convex hull plot indicating the stability of the phases from $Mg_{0/8}VS_4$ to $Mg_{8/8}VS_4$, (b) corresponding OCV for VS_4 cathode, and (c) determined mechanism of VS_4 magnesiation.

operation, we performed the studies with gradual insertion of magnesium atoms into the structure. Previous studies have shown that this material does not have a distinct location for intercalated cations, and some disorder should be expected. Thus, for each considered Mg^{2+} concentration, many possible configurations have been accounted by randomly probing different positions of Mg^{2+} inside the cathode matrix. In Fig. 2 we collect the most representative structures that help to understand the Mg^{2+} distribution patterns at different low magnesiation levels in Mg_xVS_4 (x between 0 and 0.5). We illustrate the most stable structure for each magnesiation level as a baseline, showing the relative energy of the other representative structures with respect to those of the most stable structures. Looking at the location of the single Mg^{2+}, the cation does not necessarily go to the largest cavity space between VS_4 chains, as could be expected for other cathode materials, but rather closely interacts with S_2^{2-} ligands, resulting in energy lower by 0.28 eV (Fig. 2). This is because, upon the Mg^{2+} insertion, two disulfide ligands accept four electrons, inducing the breaking of their S—S bonds. This situation could seem unbalanced from a charge neutralization point of view, i.e., one Mg^{2+} ion carries two holes while four electrons are needed to convert two disulfide ions into four S^{2-} ions. The two missing holes in the charge balance come from the Vanadium 3d band. Contrary to the electrons localized on specific disulfide ions (those closest to the inserted Mg^{2+} ion), the holes created in the V 3d band are not localized in particular V ions but are delocalized. It can be observed when looking at changes in the Bader charges (Table S2): while it is possible to clearly identify the sulfur atoms that undergo reduction (change in charge from ca. -0.35 e to ca. -1.30 e), all the vanadium cations undergo oxidation with only small differences between them (max. 0.06 e). This complex mechanism makes very favorable conditions for Mg^{2+} ions insertion, i. e., there is a very high local Coulomb interaction between the Mg^{2+} and the two broken disulfides, and the coordination becomes much more flexible by having four independent S^{2-} ligands. As the location of magnesium cation in a narrow space in between two VS_4 chains is more preferred than in a larger cavity between three VS_4 chains, one could expect preference for the interaction of Mg^{2+} in all sites of this kind. Surprisingly, we observe that the subsequent magnesium cations prefer a location close to other magnesium cations, usually doubly coordinating formed S^{2-} ligand. As shown in Fig. 2 for $Mg_{2/8}VS_4$, locating the second Mg^{2+} in an analogous site as the first one results in a 1.38 eV higher energy structure than placing the second one next to the first one. This tendency is further observed for subsequent inserted ions, as can be seen in Fig. 2, leading to some kind of aggregation of magnesium cations inside the structure. This is opposite to the homogenous location throughout the matrix, which is typically observed for cathode materials. This peculiar behavior is due to the highly localized negative region around the first inserted Mg^{2+} ion (there is a Mg^{2+} ion next to two broken disulfides, so the net local charge is −2), which further attracts subsequent magnesium cations. That overall results in the observed aggregation of Mg^{2+}, which eventually may lead to two phases in the material, poor- and rich-Mg, and thus also heterogenous mechanism of the (dis)charging.

To further explore the Mg^{2+} ions clustering, we analyzed the phase stability of the structures for different stages of magnesiation, taking the $Mg_{0/8}VS_4$ and $Mg_{8/8}VS_4$ most stable structures as a reference. The convex hull plot shows the first stable phase to be $Mg_{6/8}VS_4$ (Fig. 3a). All structures in between are unstable, and thus, they will disproportionate to $Mg_{0/8}VS_4$ and $Mg_{6/8}VS_4$. This confirms our initial findings regarding the aggregation of magnesium cations in one cathode region. Since this part of the compositional space has already been computationally studied by Wang et al. [8], we decided to take a closer look at their structures and results to compare with ours. Although Wang et al. did not analyze the phase stability using their data, based on their published energies, we were able to calculate their stability versus initial and final structures (Table S1). Indeed, similar conclusions can be drawn from that study regarding the instability of the initial phases, thereby confirming our finding.

After complete formation of $Mg_{6/8}VS_4$ phase, DFT calculations predict step-by-step intercalation of Mg^{2+}, following a homogenous solid-solution mechanism. Based on the convex hull plot, we calculate the OCV potential of VS_4 cathodes (Fig. 3b). The initial plateau, corresponding to the heterogenous two-phases separation process, matches the experimentally observed discharge plateau at 1.0 V vs. Mg during the first cycle up to around $Mg_{0.8}VS_4$ [7]. So far, the phase transition process described here has not been not detected by XRD [7]. This may be due to the high disorder of magnesium cations in the formed magnesiated phase or to kinetic effects. Thus, since the organized structure of vanadium chains does not change significantly upon intercalation of magnesium, the XRD pattern barely changes.

Further insertion of Mg^{2+} in the cathode turns the situation more complicated. We started observing a weakening of the V—S bonds,

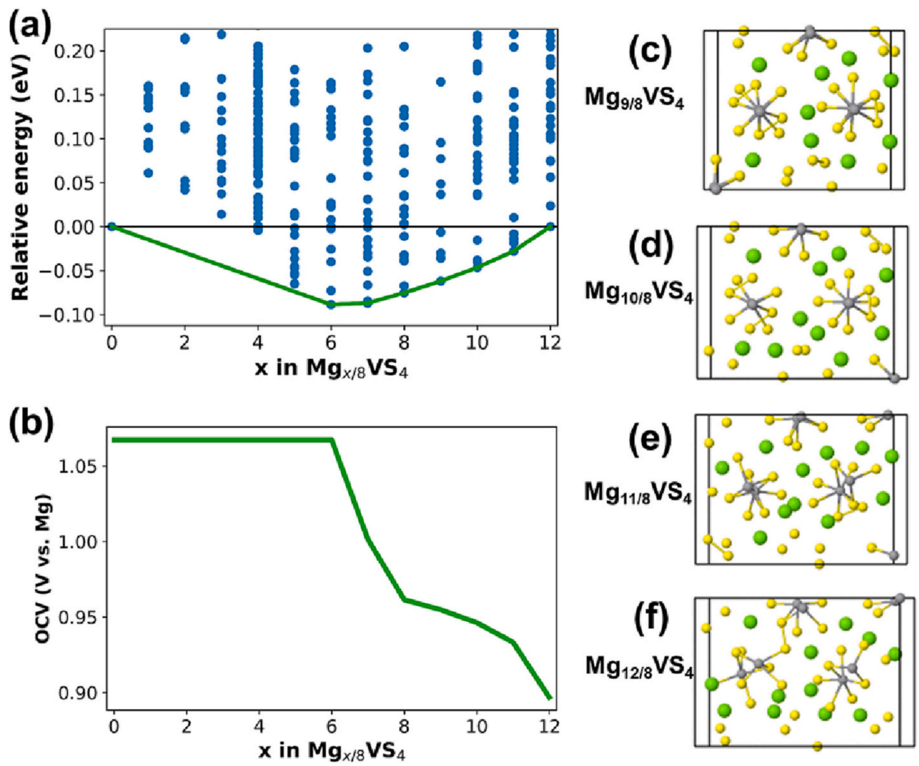

Fig. 4. (a) Convex hull plot for the composition space from $Mg_{0/8}VS_4$ to $Mg_{12/8}VS_4$, (b) corresponding OCV for VS_4 cathode and optimized the lowest energy structures of (c) $Mg_{9/8}VS_4$, (d)$Mg_{10/8}VS_4$, (e) $Mg_{11/8}VS_4$ and (f) $Mg_{12/8}VS_4$.

making them prone to dissociation. For Mg_xVS_4 structures with $x > 1$, we need to follow a special procedure during the geometry optimization. We initially blocked the possibility of the V—S bond breaking by putting Hookean spring constraint. In a second step, this constraint is released, allowing full structural relaxation. This gentle way of performing the geometry optimizations is necessary to avoid that eventual large forces at the initial guess structures may unnaturally lead to the breaking of the V—S bond(s);. It could be argued that this procedure forces the system to preserve the V—S bonds, but that is not the case since we observe situations where the V—S bond breaks, even if initially constrained. The breaking of the V—S bonds is a likely route for the degradation of the VS_4 cathode material, and below we look at this in detail. Before, we looked only at the structures preserving the V—S bonds, which are responsible for reversible charging/discharging, extending the convex hull analysis up to a concentration of $Mg_{12/8}VS_4$ (Fig. 4). The results indicate further homogenous, step-by-step intercalation of magnesium cation into the structure, at the potential around 0.9–0.95 V *vs.* Mg. The number of disulfide dimers is gradually decreasing, with finally none of them present in the lowest energy geometry of $Mg_{12/8}VS_4$. This confirms the experimentally determined limit for VS_4 cathode, which can intercalate up to 1.5 Mg per VS_4 [7]. Looking further at the structures, magnesium cations are being placed in between already present cations, highly interacting with S^{2-} ligand. Due to that, elongation of V—S bonds is observed, from 2.39 Å up to 2.56 Å, respectively for $Mg_{1/8}VS_4$ and $Mg_{12/8}VS_4$. This is accompanied by a higher negative charge at the sulfide ligand. In hypothetical, initial structure $Mg_{1/8}VS_4$ the charge present at S^{2-} has been determined to be -0.98e, and reaches a level of ca. -1.23e when going to stable $Mg_{6/8}VS_4$-$Mg_{8/8}VS_4$ phases. Further magnesiation causes a gradual increase in negative charge, with the values -1.38e, -1.52e, -1.59e and -1.61e for $Mg_{9/8}VS_4$, $Mg_{10/8}VS_4$, $Mg_{11/8}VS_4$ and $Mg_{12/8}VS_4$, respectively (Fig. S4). This induces some structural changes, which are observed in the coordination of vanadium cations: in the starting material each vanadium atom is coordinating four S_2^{2-} ligands resulting in coordination number (CN) equal 8 (Fig. S3).

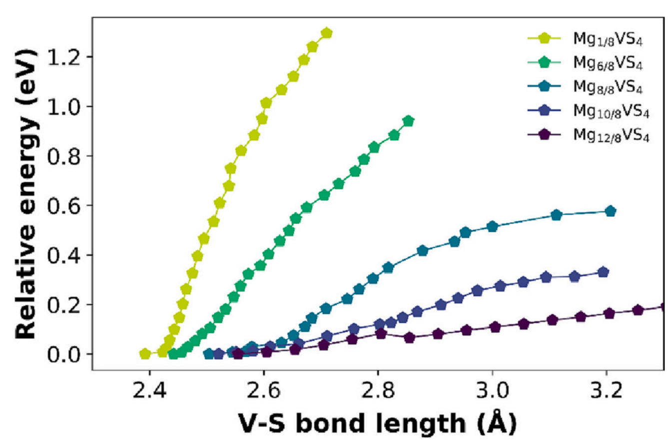

Fig. 5. Energetic profiles of the scan of the V—S bond length for different structures found with the lowest energy.

This CN is retained up to the structure $Mg_{6/8}VS_4$ even upon conversion of disulfides to sulfides. However going further, we observed slow decrease in CN towards CN = 6, as a result of detachment of co-shared sulfide anions from one of the vanadium cation, together with reformation of S_2^{2-} anions between the chains (red circle at Fig. S3d). This tendency indicates structural changes of VS_4 towards VS_2 material, where each vanadium is surrounded by 6 S^{2-} ligands. Indeed, decomposition of magnesiated phases of VS_4 towards VS_2 was confirmed by DFT to be thermodynamically preferred:

$$MgVS_4 \rightarrow MgS_2 + VS_2 \Delta E = -1.20 \text{ eV}$$

$$Mg_{1.5}VS_4 \rightarrow MgS + 0.5\ MgS_2 + VS_2 \Delta E = -1.93 \text{ eV}$$

Such degradation mechanism would involve formation of magnesium (di)sulfides inside the material, and indeed V—S bond dissociation becomes observable during geometry optimization starting from $Mg_{9/8}VS_4$. The higher negative charge at S^{2-} can be connected with lower electron donation to vanadium, thus lower bonding. To finally check how the level of magnesiation impacts the V—S bond stability, we decided to perform a scan of the V—S bonds in the lowest stable structures (Fig. 5 and S3). At each step, the distance between a single sulfur ion and vanadium ion was blocked, and the rest of the structure was optimized. The energy profiles clearly indicate the decrease of the energy needed to break the V—S bond upon increasing the concentration of magnesium, up to >5 times, when comparing $Mg_{12/8}VS_4$ to $Mg_{1/8}VS_4$. A high number of Mg^{2+} ions around a S^{2-} ligand effectively lowers the bonding between vanadium and sulfur, resulting in the sucking of sulfide by magnesium cations: it becomes energetically preferable to detach a sulfur ion from the vanadium and highly stabilize it by surrounding it with 3–4 magnesium cations. That behavior was observed for many Mg_xVS_4 structures with $x > 1$, where a higher local concentration of magnesium was present. Such a reaction leads to the formation of MgS, contributing to the lost capacity of the cathode: breaking of the V—S bond is an irreversible process.

4. Conclusions

Our theoretical analysis of the magnesation process unravels its complex nature for VS_4 cathode. Magnesium cations are intercalated in between VS_4 chains in many available sites leading to significant disorder. Moreover, the subsequent cations are not uniformly distributed, but their aggregation around the same vanadium centers is thermodynamically preferred. That leads to a phase separation towards an empty and a magnesiated phase. DFT calculations predict $Mg_{0.75}VS_4$ to be the phase formed upon initial discharging, formed at the potential of 1.07 V *vs.* Mg. That agrees well with the experimentally observed plateau at ca. 1 V vs. Mg during the initial cycle. Disordered location of magnesium cations creates flexible diffusion paths for magnesium cations, supported by sulfide ligands and shielded from vanadium-based framework [29,30]. Furthermore, our analysis explained the origin of the irreversible processes happening at a high magnesiation state: a high concentration of Mg leads to the breaking of V—S bonds and the formation of Mg—S clusters inside the cathode. This results in the experimentally observed capacity decrease by ca. 50 mAh g^{-1} after the initial cycle, together with an altered electrochemical potential profile [7]. Our previous XPS data clearly shows that after the first magnesiation, the VS_4 material never returns to its initial, pristine form [7]. Overall, our study indicates a very specific mechanism of the VS_4 magnesiation, and its knowledge together with diagnosis regarding the degradation process can lead to design of new generation VS_4 cathodes with improved properties. Doping of VS_4 material with other transitial metals, providing better stability of TM-S bond can be indicated as potentially beneficial in regard of suppressing MgS formation, and its impact on cycling stability will be a subject of subsequent studies.

CRediT authorship contribution statement

Piotr Jankowski: Conceptualization, methodology, investigation and writing of original draft.

Juan Maria Garcia Lastra: Resources, conceptualization, and review of original draft.

Declaration of competing interest

The authors declare the following financial interests/personal relationships which may be considered as potential competing interests: Juan Maria Garcia Lastra reports financial support was provided by European Union.

Data availability

Data will be made available on request.

Acknowledgements

We acknowledge the funding from the European Union's Horizon 2020 research and innovation program under grant agreement No 824066 (*E*-MAGIC).

Appendix A. Supplementary data

Supplementary data to this article can be found online at https://doi.org/10.1016/j.est.2023.106895.

References

[1] R. Mohtadi, O. Tutusaus, T.S. Arthur, Z. Zhao-Karger, M. Fichtner, The metamorphosis of rechargeable magnesium batteries, Joule 5 (3) (2021) 581–617, https://doi.org/10.1016/j.joule.2020.12.021.

[2] F. Liu, T. Wang, X. Liu, L.-Z. Fan, Challenges and recent progress on key materials for rechargeable magnesium batteries, Adv. Energy Mater. 11 (2) (2021), 2000787, https://doi.org/10.1002/aenm.202000787.

[3] R. Deivanayagam, B.J. Ingram, R. Shahbazian-Yassar, Progress in development of electrolytes for magnesium batteries, Energy Storage Mater. 21 (2019) 136–153, https://doi.org/10.1016/j.ensm.2019.05.028.

[4] M. Mao, T. Gao, S. Hou, C. Wang, A critical review of cathodes for rechargeable mg batteries, Chem. Soc. Rev. 47 (23) (2018) 8804–8841, https://doi.org/10.1039/C8CS00319J.

[5] Z. Ma, D.R. MacFarlane, M. Kar, Mg cathode materials and electrolytes for rechargeable mg batteries: a review, Batter. Supercaps 2 (2) (2019) 115–127, https://doi.org/10.1002/batt.201800102.

[6] K.R. Kganyago, P.E. Ngoepe, C.R.A. Catlow, Voltage profile, structural prediction, and electronic calculations for ${\mathrm{Mg}}_{x}{\mathrm{Mo}}_{6}{\mathrm{S}}_{8}$, Phys. Rev. B 67 (10) (2003), 104103 https://doi.org/10.1103/PhysRevB.67.104103.

[7] Z. Li, B.P. Vinayan, P. Jankowski, C. Njel, A. Roy, T. Vegge, J. Maibach, J.M. G. Lastra, M. Fichtner, Z. Zhao-Karger, Multi-electron reactions enabled by anion-based redox chemistry for high-energy multivalent rechargeable batteries, Angew. Chem. Int. Ed. 59 (28) (2020) 11483–11490, https://doi.org/10.1002/anie.202002560.

[8] Y. Wang, Z. Liu, C. Wang, X. Yi, R. Chen, L. Ma, Y. Hu, G. Zhu, T. Chen, Z. Tie, J. Ma, J. Liu, Z. Jin, Highly branched VS4 nanodendrites with 1D atomic-chain structure as a promising cathode material for long-cycling magnesium batteries, Adv. Mater. 30 (32) (2018), 1802563, https://doi.org/10.1002/adma.201802563.

[9] Z. Li, S. Ding, J. Yin, M. Zhang, C. Sun, A. Meng, Morphology-dependent electrochemical performance of VS4 for rechargeable magnesium battery and its magnesiation/demagnesiation mechanism, J. Power Sources 451 (2020), 227815, https://doi.org/10.1016/j.jpowsour.2020.227815.

[10] J.H. Chang, C. Baur, J.-M.A. Mba, D. Arčon, G. Mali, D. Alwast, R.J. Behm, M. Fichtner, T. Vegge, J.M.G. Lastra, Superoxide formation in Li2VO2F cathode material – a combined computational and experimental investigation of anionic redox activity, J. Mater. Chem. A 8 (32) (2020) 16551–16559, https://doi.org/10.1039/D0TA06119K.

[11] C. Baur, I. Källquist, J. Chable, J.H. Chang, R.E. Johnsen, F. Ruiz-Zepeda, J.-M. A. Mba, A.J. Naylor, J.M. Garcia-Lastra, T. Vegge, F. Klein, A.R. Schür, P. Norby, K. Edström, M. Hahlin, M. Fichtner, Improved cycling stability in high-capacity Li-rich vanadium containing disordered rock salt oxyfluoride cathodes, J. Mater. Chem. A 7 (37) (2019) 21244–21253, https://doi.org/10.1039/C9TA06291B.

[12] M. Arsentev, A. Missyul, A.V. Petrov, M. Hammouri, TiS3 magnesium battery material: atomic-scale study of maximum capacity and structural behavior, J. Phys. Chem. C 121 (29) (2017) 15509–15515, https://doi.org/10.1021/acs.jpcc.7b01575.

[13] S. Britto, M. Leskes, X. Hua, C.-A. Hébert, H.S. Shin, S. Clarke, O. Borkiewicz, K. W. Chapman, R. Seshadri, J. Cho, C.P. Grey, Multiple redox modes in the reversible lithiation of high-capacity, peierls-distorted vanadium sulfide, J. Am. Chem. Soc. 137 (26) (2015) 8499–8508, https://doi.org/10.1021/jacs.5b03395.

[14] B. Liu, X. Ren, J. Yin, K. Zhu, J. Yan, K. Ye, G. Wang, D. Cao, VS4 nanorods anchored graphene aerogel as a conductive agent-free electrode for high-performance lithium-ion batteries, ACS Appl. Energy Mater. 5 (1) (2022) 567–574, https://doi.org/10.1021/acsaem.1c03083.

[15] L. Wu, Y. Zhang, B. Li, P. Wang, L. Fan, N. Zhang, K. Sun, Fabrication of layered structure VS4 anchor in 3D graphene aerogels as a new cathode material for lithium ion batteries, Front. Energy 13 (3) (2019) 597–602, https://doi.org/10.1007/s11708-018-0576-9.

[16] G. Yang, B. Zhang, J. Feng, H. Wang, M. Ma, K. Huang, J. Liu, S. Madhavi, Z. Shen, Y. Huang, High-crystallinity urchin-like VS4 anode for high-performance lithium-ion storage, ACS Appl. Mater. Interfaces 10 (17) (2018) 14727–14734, https://doi.org/10.1021/acsami.8b01876.

[17] Y. Zhou, J. Tian, H. Xu, J. Yang, Y. Qian, VS4 nanoparticles rooted by A-C coated MWCNTs as an advanced anode material in lithium ion batteries, Energy Storage Mater. 6 (2017) 149–156, https://doi.org/10.1016/j.ensm.2016.10.010.

[18] S. Wang, W. Ma, X. Zang, L. Ma, L. Tang, J. Guo, Q. Liu, X. Zhang, VS4-decorated carbon nanotubes for lithium storage with pseudocapacitance contribution, ChemSusChem 13 (6) (2020) 1637–1644, https://doi.org/10.1002/cssc.201901412.

[19] X. Xu, S. Jeong, C.S. Rout, P. Oh, M. Ko, H. Kim, M.G. Kim, R. Cao, H.S. Shin, J. Cho, Lithium reaction mechanism and high rate capability of VS4–graphene nanocomposite as an anode material for lithium batteries, J. Mater. Chem. A 2 (28) (2014) 10847–10853, https://doi.org/10.1039/C4TA00371C.

[20] L. Luo, J. Li, H. Yaghoobnejad Asl, A. Manthiram, In-situ assembled VS4 as a polysulfide mediator for high-loading lithium-sulfur batteries, ACS Energy Lett. 5 (4) (2020) 1177–1185, https://doi.org/10.1021/acsenergylett.0c00292.

[21] P. Jing, H. Lu, W. Yang, Y. Cao, B. Xu, W. Cai, Y. Deng, Polyaniline-coated VS4@rGO nanocomposite as high-performance cathode material for magnesium batteries based on Mg2+/Li+ dual ion electrolytes, Ionics 26 (2) (2020) 777–787, https://doi.org/10.1007/s11581-019-03239-3.

[22] G. Kresse, J. Hafner, Ab initio molecular dynamics for liquid metals, Phys. Rev. B 47 (1) (1993) 558–561, https://doi.org/10.1103/PhysRevB.47.558.

[23] J. Sun, A. Ruzsinszky, J.P. Perdew, Strongly constrained and appropriately normed semilocal density functional, Phys. Rev. Lett. 115 (3) (2015), 036402, https://doi.org/10.1103/PhysRevLett.115.036402.

[24] P.E. Blöchl, Projector augmented-wave method, Phys. Rev. B 50 (24) (1994) 17953–17979, https://doi.org/10.1103/PhysRevB.50.17953.

[25] Z. Rong, D. Kitchaev, P. Canepa, W. Huang, G. Ceder, An efficient algorithm for finding the minimum energy path for cation migration in ionic materials, J. Chem. Phys. 145 (7) (2016), 074112, https://doi.org/10.1063/1.4960790.

[26] A. Anelli, E.A. Engel, C.J. Pickard, M. Ceriotti, Generalized convex hull construction for materials discovery, Phys. Rev. Mater. 2 (10) (2018), 103804, https://doi.org/10.1103/PhysRevMaterials.2.103804.

[27] M.K. Beyer, The mechanical strength of a covalent bond calculated by density functional theory, J. Chem. Phys. 112 (17) (2000) 7307–7312, https://doi.org/10.1063/1.481330.

[28] W. Tang, E. Sanville, G. Henkelman, A grid-based Bader analysis algorithm without lattice bias, J. Phys. Condens. Matter 21 (8) (2009), 084204, https://doi.org/10.1088/0953-8984/21/8/084204.

[29] S. Rubio, R. Ruiz, W. Zuo, Y. Li, Z. Liang, D. Cosano, J. Gao, Y. Yang, G.F. Ortiz, Insights into the reaction mechanisms of nongraphitic high-surface porous carbons for application in Na- and mg-ion batteries, ACS Appl. Mater. Interfaces 14 (38) (2022) 43127–43140, https://doi.org/10.1021/acsami.2c09237.

[30] S. Rubio, Z. Liang, X. Liu, P. Lavela, J.L. Tirado, R. Stoyanova, E. Zhecheva, R. Liu, W. Zuo, Y. Yang, C. Pérez-Vicente, G.F. Ortiz, Reversible multi-electron storage enabled by Na5V(PO4)2F2 for rechargeable magnesium batteries, Energy Storage Mater. 38 (2021) 462–472, https://doi.org/10.1016/j.ensm.2021.03.035.